JOURNAL OF THERMOPHYSICS AND HEAT TRANSFER
Vol. 8, No. 3, July–Sept. 1994

Void Profiles in Unidirectional Solidification: The Role of Capillary Forces and Gravity

C. D. Sulfredge,* K. A. Tagavi,† and L. C. Chow‡
University of Kentucky, Lexington, Kentucky 40506

Some of the effects of capillary forces and the solid-liquid contact angle have been incorporated into previously known solutions for solidification shrinkage void profiles. Comparisons are then drawn between the original profiles from the literature and the modified capillary result. Since the capillary rise is a function of the gravitational acceleration, the new solution could also be extended down to reduced gravity conditions. We feel these results will lead to a better understanding of solidification shrinkage void shapes in a variety of circumstances.

Nomenclature

A = meniscus cross-sectional area
H = chamber height
h = capillary rise height
L = chamber length
L_c = capillary characteristic length, Eq. (8)
R = chamber radius
r = radial coordinate
V = volume
x = Cartesian length coordinate
y = Cartesian height coordinate
z = cylindrical height coordinate
γ = solidification shrinkage fraction, $1 - \rho_l/\rho_s$
θ = solid-liquid contact angle
ρ = mass density
σ = surface tension

Subscripts
c = characteristic
cent = centroid
fm = fixed mass
l = liquid
s = solid

Introduction

ALTHOUGH phase change processes such as melting or freezing are a familiar part of everyday life, closer examination reveals some subtle complexities of which many are unaware. For instance, Chalmers[1] presents a fascinating discussion showing how such diverse phenomena as the hexagonal form of snowflakes and the separation of electric charge in a thunderhead are related to the process by which water freezes. Another interesting and poorly understood aspect of the solidification process concerns disposition of the volume change accompanying the phase transition.

A change of phase always coincides with a change in density as the molecules rearrange into a new atomic structure.[2] In water, the solid phase has a more open crystal lattice than the liquid. Thus, ice is less dense than water, and a water-ice mixture will expand in volume as freezing proceeds. On the other hand, the solid phase is denser than the liquid for almost all other substances. Hence, solidification of these materials will always be accompanied by a decrease in overall volume. Regrettably, such behavior can have unfortunate consequences to the integrity of the solidified material.

Work on the prediction of final void shapes in the solid dates back many years. Many of these results are products of the foundry industry, as metallurgists strove to devise techniques for producing castings free from shrinkage-induced defects. Knowledge of the "pipe" profiles assumed by solidification shrinkage voids allows additional reservoirs of molten metal known as risers to be incorporated into the mold. As long as the shrinkage pipe is contained entirely within a riser, it can be removed by machining to produce a sound casting. With this objective in mind, simple analytical solutions have been developed for the ultimate shape of the shrinkage voids formed during unidirectional solidification of various ingot geometries.[3,4] Analytical and numerical results are also available for void profiles in a few other solidification cases. Sulfredge et al.[2] developed an analytical solution including the contact angle for the interface shape during radial solidification of a long tube in $0g$. Morris et al.[5] have also solved for the void profile inside a spherical container of liquid by assuming a preferred location for the shrinkage to appear and applying a Runge-Kutta scheme to the capillary differential equation for the interface. Finite difference solutions of the heat diffusion equation combined with a volume accounting procedure have been developed by both Shamsundar and Sparrow[6] and Wichner et al.[7] However, none of these studies fully incorporates the interrelated factors of gravitational forces, capillary forces, and the solid-liquid contact angle.

This article will attempt to expand upon the solidification profile results already published by Chalmers.[3] Initially, his previously known solutions for overall void profiles in unidirectional solidification will be generalized to include the combined effects of capillary forces and the solid-liquid contact angle in hopes of achieving a more realistic model. The results will also be adjusted to yield profiles appropriate under reduced-gravity conditions. Hopefully, studying the void-formation mechanism under these relatively idealized circumstances will provide insight into more complex solidification cases.

Analysis Neglecting Capillary Forces

Two common geometries of unidirectional freezing examined by Chalmers[3] to predict the solidification shrinkage void profiles are illustrated in Fig. 1. Figure 1a corresponds to unidirectional freezing from the left for a rectangular container of dimensions L and H which is long in the z direction, while Fig. 1b depicts radial solidification for a cylinder with

Received May 3, 1993; revision received Aug. 24, 1993; accepted for publication Aug. 25, 1993.

*Ph.D. Candidate, Department of Mechanical Engineering. Member AIAA.
†Associate Professor, Department of Mechanical Engineering.
‡Professor, Department of Mechanical Engineering. Member AIAA.

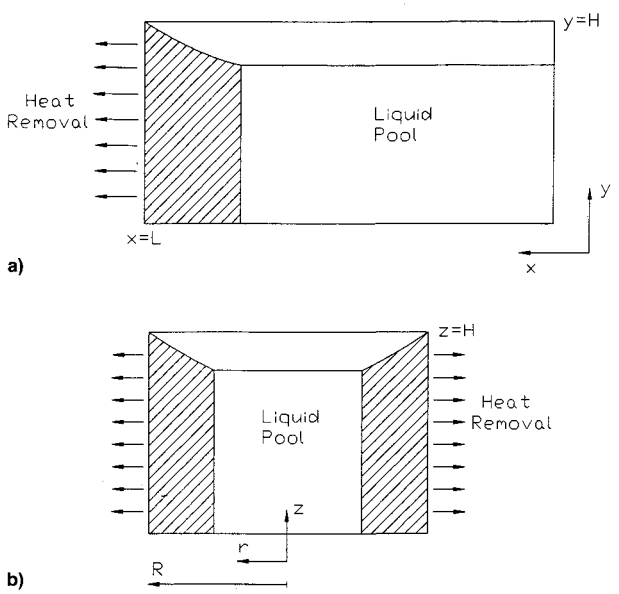

Fig. 1 Intermediate stage of the unidirectional solidification process for a) Cartesian and b) radial geometries, with capillary effects neglected.

measurements H and R. By symmetry, the Fig. 1a Cartesian result is also valid for freezing a container of length $2L$ from both ends. For both situations, gravity acts downward along the axis of the height dimension and the container is initially filled with liquid. A closed-form, analytical solution is possible in either geometry if one assumes the solidification front is always vertical and the liquid phase pools in the lowest available part of the container. In addition to these assumptions, profiles available in the literature also neglect the effects of surface tension forces by assuming a planar liquid surface with no capillary rise at the solid-liquid interface, although it will be shown later that such effects can be successfully incorporated into the model. All such solutions are based on a volumetric accounting procedure with no consideration of the void nucleation process.

Performing an overall mass balance on the two-dimensional Cartesian geometry from Fig. 1a yields

$$\int_x^L \rho_s y(\xi)\, d\xi + \rho_l y x = \rho_l H L \tag{1}$$

where $y(x)$ represents the uppermost point of the freezing front as a function of x, and therefore traces out the void interface profile. In Eq. (1), x is the independent variable tracking the interface position, and ξ is a dummy variable of integration with $x \le \xi \le L$, while ρ_s and ρ_l stand for the solid and liquid densities. The two terms on the left side of the equation represent the mass of phase change material (PCM) in the solid and liquid phases at some intermediate step in the freezing process, and the right side represents the total mass initially present. Differentiating the overall mass balance with respect to x gives a differential equation for the void interface shape $y(x)$:

$$-\rho_s y + \rho_l x \frac{dy}{dx} + \rho_l y = 0 \tag{2}$$

Equation (2) can be simplified by defining the solidification shrinkage fraction $\gamma = 1 - \rho_l/\rho_s$, which represents the ratio of the final void volume to the total volume of the container. Expressed in terms of γ, Eq. (2) becomes

$$\frac{\gamma}{1-\gamma} y\, dx = x\, dy \tag{3}$$

Separating variables and integrating subject to the initial condition $y(x = L) = H$ yields the void profile for this Cartesian geometry:

$$y/H = (x/L)^{\gamma/(1-\gamma)} \tag{4}$$

A similar integral mass accounting on the radial geometry of Fig. 1b requires

$$\int_r^R \rho_s z(\xi) 2\pi\xi\, d\xi + \rho_l \pi r^2 z = \rho_l \pi R^2 H \tag{5}$$

where $z(r)$ stands for the locus of all the topmost points on the solid-liquid interface over the course of the solidification process in cylindrical coordinates. Here, r is the independent parameter, and ξ is again a dummy variable which ranges over the interval of integration such that $r \le \xi \le R$. Differentiating, introducing the shrinkage fraction γ, and solving subject to $z(r = R) = H$ gives the radial void profile

$$z/H = (r/R)^{2\gamma/(1-\gamma)} \tag{6}$$

The solution profiles obtained with various values of γ are sketched in Fig. 2a for the Cartesian geometry, and Fig. 2b for the case of radial solidification. A γ value of 7.79% is characteristic of cyclohexane, a cyclic-structured hydrocarbon previously used in experiments to model solidification shrinkage,[8] while $\gamma = 35\%$ corresponds to the LiH phase change material utilized by several other investigators.[5] Apparently

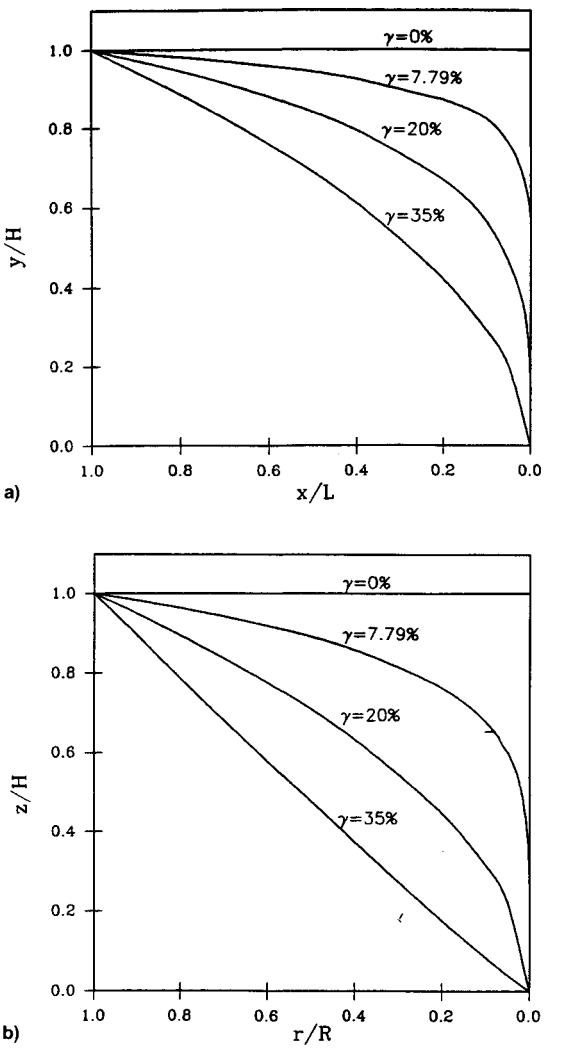

Fig. 2 a) Cartesian and b) radial coordinate void profiles for γ = 0, 7.79, 20, and 35% from Chalmers's solutions.

changing the solidification shrinkage fraction has little effect on the general form of the solution. In both the radial and Cartesian cases, the void penetrates to the container bottom regardless of the value of γ and exhibits a cusp at this point. Both these characteristics of the published void profiles physically seem rather unrealistic in light of the capillary forces implied by Laplace's equation, which states that the capillary pressure differential across the liquid-vapor interface is inversely proportional to the radius of curvature, when the radius of curvature goes to zero at the cusp. Thus, formation of such a cusp profile would imply an infinite capillary force. Incorporation of capillary considerations and the solid-liquid contact angle into the model should help eliminate this difficulty and produce a more reasonable estimate of the final void shape.

Analysis Including Capillary Effects

The analytical void-profile solutions for unidirectional solidification just obtained are based on some assumptions which are physically unrealistic. A uniform vertical freezing front can at least be approached in a carefully controlled experiment if γ is not so large that the interface area varies greatly during the course of solidification and introduces a significant two-dimensional character to the solution. Furthermore, the remaining liquid would collect at the bottom of the container under any appreciable gravitational acceleration. However, the liquid-free surface will never be planar due to the capillary rise present at the solid-liquid interface. The upcoming analysis will incorporate capillary rise and the presence of a wetting contact angle in hopes of obtaining a more realistic solution profile.

An intermediate stage in the unidirectional solidification of a rectangular container analogous to that in Fig. 1a, but including the presence of a capillary meniscus at the vertical freezing front, is illustrated in Fig. 3. Figure 4 shows a close-up of the capillary rise and its relationship to the contact angle θ. Carey[9] has already presented a solution for the interface profile $y(z)$ in Fig. 4 as

$$y(z) = L_c\left[\cosh^{-1}\left(\frac{2L_c}{z}\right) - \cosh^{-1}\left(\frac{2L_c}{h}\right) + (4 + h^2/L_c^2)^{1/2} - (4 + z^2/L_c^2)^{1/2}\right] \tag{7}$$

where L_c is a characteristic length defined by

$$L_c = \left[\frac{\sigma}{(\rho_l - \rho_s)g}\right]^{1/2} \tag{8}$$

and h is the capillary rise at the interface. From a capillary force balance adjacent to the wall, one obtains the relation[9]

$$h = \left[\frac{2\sigma(1 - \sin\theta)}{(\rho_l - \rho_s)g}\right]^{1/2} \tag{9}$$

in which σ is the liquid surface tension, θ represents the contact angle at the interface, and g stands for the acceleration of gravity.

Once capillary effects are included into Fig. 3, the overall mass balance becomes

$$\int_x^L \rho_s y(\xi)\, d\xi + \rho_l(y - h)x + \rho_l A_{\text{meniscus}} = \text{Total PCM mass/unit depth} \tag{10}$$

where A_{meniscus} represents the cross-sectional area accommodated in the capillary meniscus, as shown by the vertically striped area in Fig. 3. Fortunately Carey's solution shows that

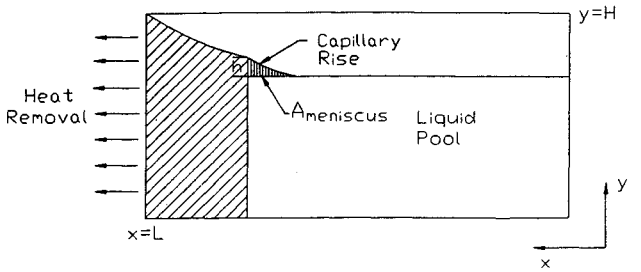

Fig. 3 Intermediate step in the solidification process for a Cartesian geometry, including the capillary meniscus.

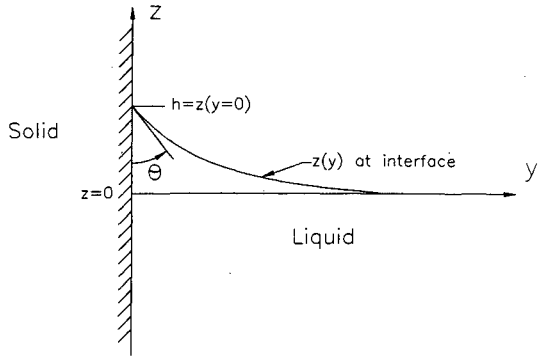

Fig. 4 Close-up of the capillary rise at the solid-liquid interface and its relationship to the contact angle.

A_{meniscus} is a constant, unless system dimensions become less than the characteristic length L_c. Equation (10) differs from Eq. (1) in that some liquid PCM is tied up in the meniscus, and the liquid pool now lies at a lower level than point $y(x)$ on the current solidification interface for any value of x.

Differentiating Eq. (10) with respect to x yields the void profile differential equation adjusted for capillary considerations:

$$-\rho_s y + \rho_l\left(x\frac{dy}{dx} + y - h\right) = 0 \tag{11}$$

If one introduces the shrinkage fraction γ and simplifies algebraically, the equation becomes

$$\frac{dy}{dx} - \left(\frac{\gamma}{1 - \gamma}\right)\frac{y}{x} = \frac{h}{x} \tag{12}$$

Solving subject to the initial condition $y(x = L) = H$ yields the final void profile as

$$y/H = (x/L)^{\gamma/(1-\gamma)} + \frac{h}{H[\gamma/(1 - \gamma)]}\left[(x/L)^{\gamma/(1-\gamma)} - 1\right] \tag{13}$$

after converting to normalized form.

An interesting special case of the contact-angle solution for unidirectional freezing in a Cartesian geometry is the case of $\gamma = 0$, or no shrinkage taking place upon solidification. For the traditional solution by Chalmers from Eq. (4), $\gamma = 0$ would correspond to a normalized profile of $y/H = 1$. However, the liquid level would be forced downward by the capillary meniscus, even though no shrinkage was occurring. The final void profile for such a situation can be found by letting $\gamma \to 0$ in Eq. (13), but this technique would require using L'Hopital's rule to evaluate an indeterminate expression of the form ∞*0. A simpler approach is to set $\gamma = 0$ in Eq. (12) and solve the resulting differential equation

$$\frac{dy}{dx} = \frac{h}{x} \tag{14}$$

subject to the initial condition $y(x = L) = H$. Carrying out these calculations yields the normalized profile

$$y/H = 1 - (h/H)^{1/4}(L/x) \tag{15}$$

Both Eq. (13) and Eq. (15) contain the solutions of Chalmers, since setting $h = 0$ immediately recovers the results which neglect capillary effects. Such a situation corresponds to a contact angle of $\theta = 90$ deg in Eq. (9), but contact angles close to zero are much more common in practical applications. The additional solution terms resulting from values of $h \neq 0$ also give the void profile solutions a somewhat different mathematical character. For instance, it is clear that in Eq. (13) $y(x)$ will go to zero for some value of $x > 0$, and this point of contact with the chamber bottom will depend on γ as well as h and H. On the other hand, the original solution for $y(x)$ from Eq. (4) never went to zero except for $x = 0$, regardless of the value of γ. The capillary height h also depends on the contact angle and the force of gravity. Obviously, such things can lead to a considerably different interface shape from Chalmers's solution for the right combination of parameters. Hence, the overall impact of the additional capillary factors on the void profiles can only be gauged in terms of some numerical examples for different shrinkage fractions and gravitational accelerations. Like Chalmers's Cartesian solutions, these results can also be viewed as one side of a symmetric void profile for a solidification cell of length $2L$ frozen from both ends.

Figure 5 illustrates the effect of changing γ on both the original and generalized void profile solutions and also allows comparison of the two results for the same amount of shrinkage. These profiles were calculated using the thermophysical properties of cyclohexane,[10] which yielded an h value of 2.63 mm under 1g. Chamber measurements of $H = 2$ cm and $L = 5$ cm were assumed since they are similar to the dimensions of the LiH canisters studied by Morris.[5] Results were obtained for $\gamma = 7.79\%$ (the cyclohexane value), $\gamma = 35\%$ (the largest amount of shrinkage typically observed in PCMs), and an intermediate value of $\gamma = 20\%$. The situation where the original and generalized solutions were compared for specified PCM masses, rather than for equivalent canister dimensions, would be very similar and is discussed in the Appendix.

Clearly, the new capillary solution always lies below Chalmers's result for an equivalent sized PCM container, and the void profiles shift downward to accommodate a larger void with increasing γ. Part of the shift results from the smaller

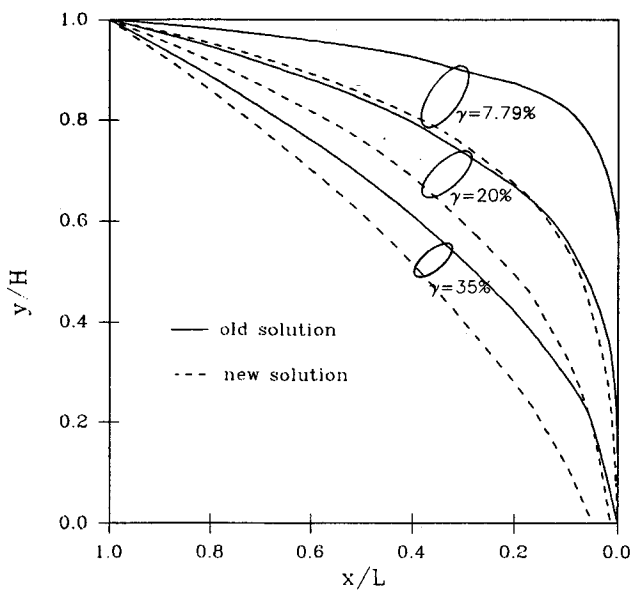

Fig. 5 Capillary solution void profiles for a Cartesian geometry under 1g with $\gamma = 7.79$, 20, and 35%.

total mass of PCM required to fill a container of height H when a capillary meniscus is initially present, and the remainder is due to the influence of capillary forces during solidification. However, the discrepancy between the two solutions appears to become more pronounced at larger values of the solidification shrinkage fraction. The new capillary solution reached the container bottom at larger values of x/L as γ increased, but this contact point remained quite close to $x = 0$, even for large values of γ. Furthermore, the solution profile now had a finite slope when it reached the bottom of the PCM canister and no longer exhibited the cusp form with a vertical tangent line which characterized Chalmers's result.

The effect of reduced gravitational acceleration on the solution profiles was also examined, and the resulting curves are plotted in Fig. 6. Calculations have been performed for gravitational fields of $\frac{1}{2}$ g and $\frac{1}{10}$ g for comparison with the previous 1 g results. The older solution is completely independent of gravitational effects, as evident from the lack of any gravity parameters in Eq. (4). On the other hand, the new results show a marked variance under reduced gravity, especially at $\frac{1}{10}$ g. As the gravitational acceleration was reduced, the solution profile shifted downward and the x coordinate at which it intercepted the chamber bottom increased. These effects were due to changes in h, which varies as $g^{-1/2}$. Using cyclohexane property data, $\frac{1}{2}$ g corresponds to $h = 3.73$ mm, while $\frac{1}{10}$ g yields $h = 8.35$ mm or about 42% of the chamber height in this example.[10]

Perhaps the most striking difference between Chalmers's solutions and the new capillarity result is illustrated by the data graphed in Fig. 7 for several different gravity values with $\gamma = 0$. The older result predicts a planar interface with $y = H$, even under microgravity conditions. In contrast, the generalized result indicates a curved profile resulting from the liquid pool lying below the top of the freezing front. Such effects can impart considerable amounts of curvature to the void interface when h is large, as illustrated by the $\frac{1}{10}$ g profiles from Fig. 7.

Incorporation of capillary effects into Chalmers's solution for a radial geometry is also possible, but results in a somewhat more complex equation than encountered in the Cartesian case. Figure 8 depicts the solidification process in this geometry with the freezing front located at some arbitrary radius r and a capillary meniscus rise of h present at the interface. The container has dimensions H and R, with the void profile represented as $z(r)$. An overall mass accounting requires

$$\rho_s \int_r^R 2\pi\xi z(\xi)\, d\xi + \rho_l V_{\text{meniscus}} + \rho_l \pi(z - h)r^2 = \text{Total PCM mass} \tag{16}$$

where V_{meniscus} stands for the volume subtended by the capillary rise stretching around the circumference of the liquid pool. The cross-sectional area occupied by this volume has been marked with vertical stripes in Fig. 8. Now by the theorem of Pappus,[11] V_{meniscus} can be related to the area under the capillary profile and the radius of revolution by

$$V_{\text{meniscus}} = 2\pi r_{\text{cent}} A \tag{17}$$

in which A is the meniscus cross-sectional area, and r_{cent} is the radius traveled by the centroid in tracing out the solid of revolution. The meniscus area is readily obtained by integrating Carey's one-dimensional meniscus profile to yield

$$A = L_c\left\{2L_c \sin^{-1}\left(\frac{h}{2L_c}\right) + \frac{h}{2}(4 + h^2/L_c^2)^{1/2} + 2L_c/\left[\frac{2}{h/L_c + (4 + h^2/L_c^2)^{1/2}}\right]\right\} \tag{18}$$

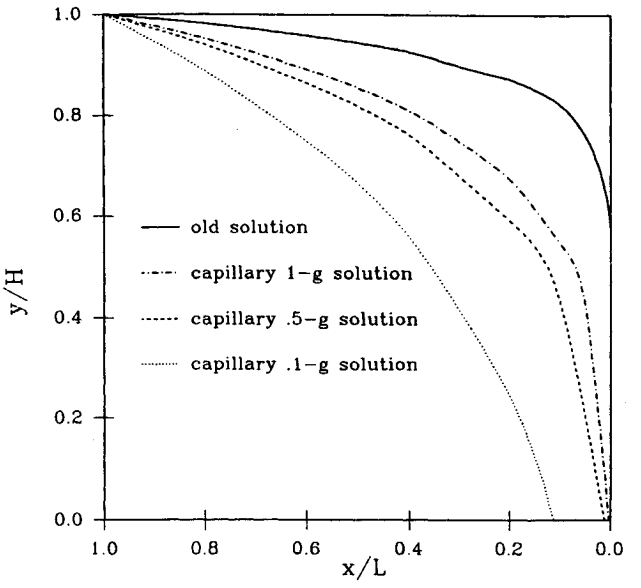

Fig. 6 Capillary solution void profiles for a Cartesian geometry with $\gamma = 7.79\%$ and various gravitational accelerations.

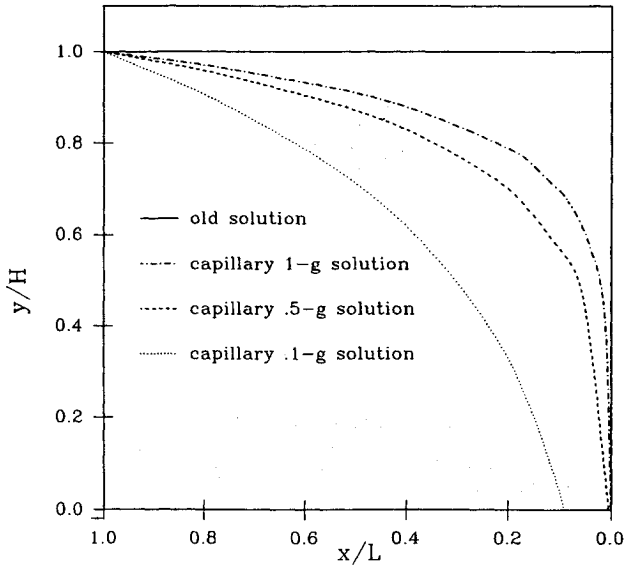

Fig. 7 Capillary solution void profiles for a Cartesian geometry with $\gamma = 0\%$ and various gravitational accelerations.

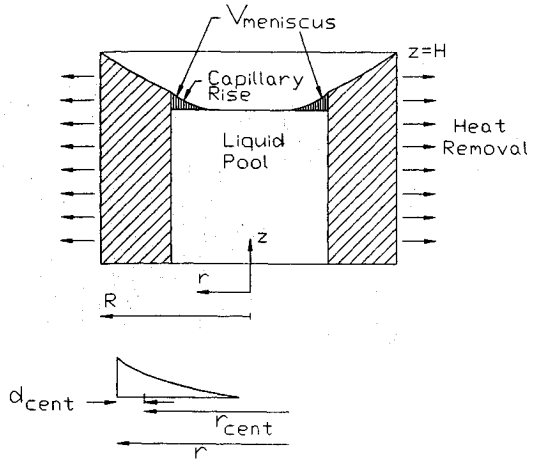

Fig. 8 Intermediate step in the solidification process for a radial geometry, including the capillary meniscus.

As shown by the inset drawing in Fig. 8, r_{cent} will be related to the solidification front radius by some constant factor d_{cent} that locates the centroid of the meniscus cross section. Hence

$$r = r_{cent} + d_{cent}(\text{const}) \tag{19}$$

Substituting Eqs. (17) and (19) into Eq. (16) then yields

$$\rho_s \int_r^R 2\pi\xi z(\xi)\, d\xi + \rho_l A 2\pi(r - d_{cent}) + \rho_l \pi(z - h)r^2 = \text{Total PCM mass} \tag{20}$$

Differentiating Eq. (20) with respect to r results in the governing differential equation for the void interface profile:

$$-\rho_s 2\pi rz + 2\rho_l \pi A + \rho_l \pi r^2 \frac{dz}{dr} + 2\rho_l \pi zr - 2\rho_l \pi hr = 0 \tag{21}$$

Introducing γ and integrating subject to $z(r = R) = H$, yields the normalized void profile:

$$z/H = (r/R)^{2\gamma/(1-\gamma)} + \frac{h}{H[\gamma/(1-\gamma)]}[(r/R)^{2\gamma/(1-\gamma)} - 1] + \frac{2A}{[1 + 2\gamma/(1-\gamma)]RH}[(r/R)^{-1} - (r/R)^{2\gamma/(1-\gamma)}] \tag{22}$$

Like the Cartesian capillary result, it is possible to obtain a solution for the no shrinkage case by setting $\gamma = 0$ prior to solving the differential equation. The radial solution analogous to Eq. (15) is then

$$z/H = 1 - \frac{2h}{H}\ln(R/r) + \frac{2A}{RH}[(r/R)^{-1} - 1] \tag{23}$$

The first terms of Eqs. (22) and (23) therefore reproduce Chalmers's radial solidification results, while the remainder of each equation represents higher-order effects due to capillary forces. Once again, numerical examples must be considered to assess the impact of these terms on the character of the solution.

The numerical results obtained in the radial geometry for solidification shrinkage fractions of $\gamma = 7.79$, 20, and 35% under a gravity field of 1g have been plotted in Fig. 9. Con-

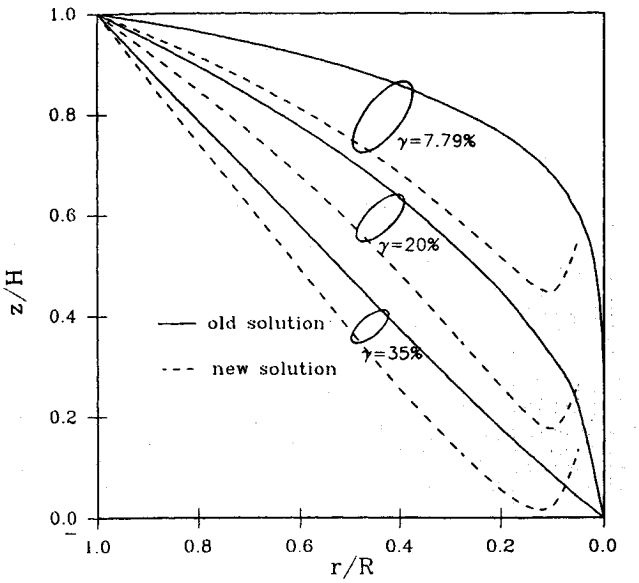

Fig. 9 Capillary solution void profiles for a radial geometry under 1 g with $\gamma = 7.79$, 20, and 35%.

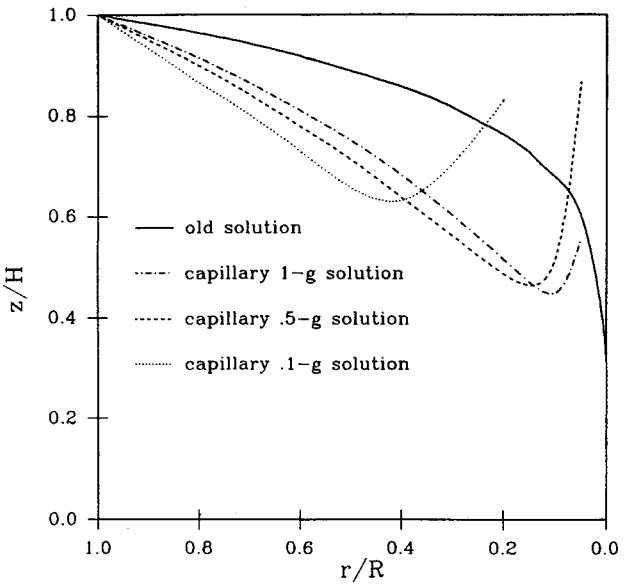

Fig. 10 Capillary solution void profiles for a radial geometry with γ = 7.79% and various gravitational accelerations.

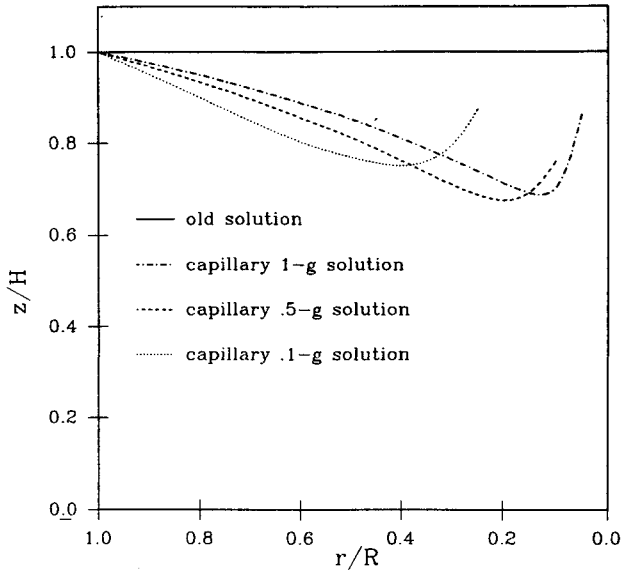

Fig. 11 Capillary solution void profiles for a radial geometry with γ = 0% and various gravitational accelerations.

tainer dimensions of $R = H = 2$ cm were assumed, and cyclohexane's property data[10] yielded $A = 6.8704 \times 10^{-6}$ m^2 for standard gravity conditions. Both Chalmers's original solution and the generalized result are included for comparison purposes. Readers interested in the changes to this solution required for the specified PCM mass case should refer to the Appendix. Near the container wall, the newer profile tends to lie below the previous approximation as was observed with a Cartesian geometry. This effect again results from both a smaller initial mass of PCM due to the original meniscus at the top of the container and the impact of the new capillary terms on the solution profile. However, including capillary effects caused the void shape $z(r)$ to increase again for r/R less than about 0.1. In fact, the solution for $z(r)/H$ actually tends toward infinity as r approaches zero due to the $(r/R)^{-1}$ term in Eq. (22). Of course, such behavior at small values of r/R is physically unrealistic, but it illustrates the dominating effect of capillary forces in the final stage of solidification.

The capillary solution void profile curves for a shrinkage fraction of 7.79% under $\frac{1}{2}$ g and $\frac{1}{10}$ g are plotted in Fig. 10 for comparison with the 1g solution. Under $\frac{1}{2}$ g, the meniscus area term increased to 1.3741×10^{-5} m^2, while $\frac{1}{10}$ g led to an A

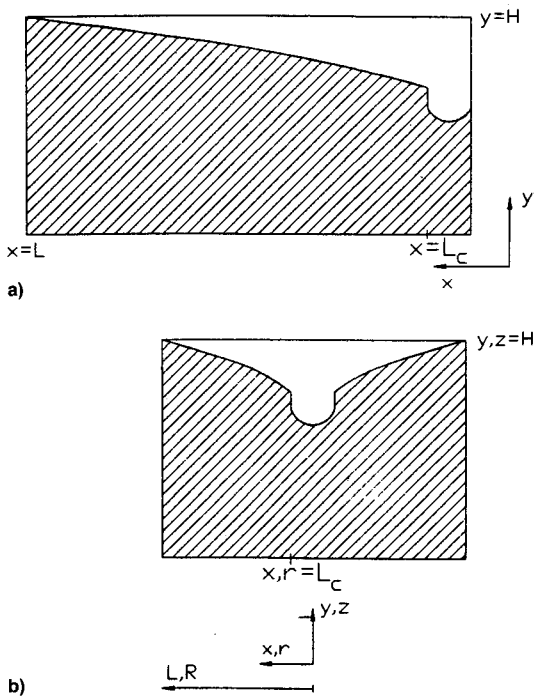

Fig. 12 General form of the capillary solution void profiles corrected to take L_c into account in a) unidirectional Cartesian freezing and b) symmetric Cartesian or radial solidification.

value of 6.8704×10^{-5} m^2. Since more liquid was included in the capillary rise at each stage of solidification, one would expect greater deviation from the Chalmers's solution under reduced gravity conditions. This trend is clearly evident in Fig. 10. At $\frac{1}{10}$ g, the profile began tending upward to form a central peak near $r/R = 0.4$, and for $\frac{1}{2}$ g conditions this phenomenon appeared at about $r/R = 0.2$. However, under normal gravity, upward void growth was delayed until almost $r/R = 0.1$, because of the smaller meniscus area and capillary rise characteristic of these conditions.

Like the rectangular coordinate solidification case already considered, capillary effects lead to a massive deviation from Chalmers's results when $\gamma = 0$. To highlight the differences between the solutions, the interfacial profile results for radial solidification with no shrinkage are shown in Fig. 11. Instead of $Z = H$ for all values of r, one now has a profile which is initially pipe-like and then tends to infinity near $r = 0$. Decreasing the acceleration of gravity had precisely the same effect seen with nonzero γ, since the capillary rise and meniscus area were both magnified relative to container height. Even more than for cases with nonzero γ, it is clear that one must take into account capillary forces in order to obtain a realistic profile when essentially no shrinkage is present.

Since the capillary adjusted profiles still resulted in voids always reaching the chamber floor in a Cartesian geometry and caused the radial profile to exhibit a singularity at its central axis, one might question whether they represent a significant advance over the previous work. However, the cusp shape with its accompanying vertical tangent line at $x = 0$ has been eliminated from the rectangular coordinate profile. These achievements do bring the solidification model closer to physical reality. But perhaps the most important contribution resulting from the inclusion of capillary forces is the establishment of a minimum characteristic length scale for the solidification process.

On a fundamental level, both Chalmers's work and the differential equations modified with capillary terms suffer from the same drawback: the assumption that the liquid pool can be infinitely subdivided along the x or r axes near the origin without changing the forces acting on a fluid element. This idea is implied whenever one speaks of a governing differential equation that remains valid for arbitrarily small values

of x or r. However, capillary forces resulting from Laplace's equation have given rise to a characteristic length L_c, as defined by Eq. (8) in terms of fluid properties and the force of gravity. Once the solidification front reaches a point with x or $r < L_c$, the governing differential equation will no longer represent the physics acting on the remaining liquid any more than Chalmers's equations neglecting capillary did. This problem accounts for the continued void penetration to the chamber bottom and the growth toward infinity that occur when the axial coordinates become less than L_c.

To correct the difficulty, one should probably follow the capillary solution curve instead of Chalmers's result until x or $r = L_c$, and then accommodate the remaining solidification shrinkage by simple vertical subsidence of the surviving liquid column. Such a procedure would produce a void profile of the form illustrated in Fig. 12a for the Cartesian case with solidification from one end. In solidifying a rectangular geometry of length $2L$ from both ends or for radial solidification, one would obtain the general form depicted in Fig. 12b. These void profiles are very similar to the shrinkage pipes obtained experimentally by Ohno[12] for solidification of aluminum and titanium ingots. This approach seems the simplest way to deal with the problem of dendritic growth bridging the liquid pool and the two-dimensional heat transfer effects which will appear when the final liquid column becomes extremely narrow. One must also note that L_c is a function of g, so that the final pipe will have a greater size in microgravity conditions.

One other interesting aspect of the new capillary solutions is their lack of dimensional scalability. In Chalmers's original work

$$y/H = f\left(\frac{x}{L}, \frac{\gamma}{1-\gamma}\right)$$

for a Cartesian geometry and

$$z/H = g\left(\frac{r}{R}, \frac{\gamma}{1-\gamma}\right)$$

for a radial geometry. Thus, both solutions depended on only two normalized parameters, and the profile results were fully scalable to any container size. Regardless of H, the normalized profiles would be identical for equal values of γ. However, the modified capillary solutions have introduced one new dimensionless group to the Cartesian solution and two more to the radial result. As one can readily see from Eqs. (13) and (15), the Cartesian profile now depends on h/H as well as the two previous parameters. Similarly, the radial profiles in Eqs. (22) and (23) now involve the dimensionless groups h/H and A/RH in addition to those from Chalmers's results.

The presence of these new groups in the capillary void profiles destroys the perfect dimensional scalability that used to be present. The chamber dimensions can no longer be scaled out because they now enter the capillary solutions relative to the quantities h and A which are fixed by fluid properties and the gravitational acceleration. Now changing H or R would alter the value of h/H or A/RH and change the shape of the void profile for the new container size. Naturally, the new capillary terms have their greatest influence on the void profile when the chamber dimensions are of the same order of magnitude as the characteristic capillary height and meniscus area. As H tends toward infinity, both of the new capillary parameters approach zero, and their influence on the solution declines. Therefore, by freezing a very deep bath of liquid in either a radial or Cartesian geometry, one would recover Chalmers's solution for unidirectional solidification even though θ was not equal to 90 deg.

Hopefully, the preceding improvements on older unidirectional solidification results will contribute to a greater understanding of the void formation process in general, as well as the specific effects of gravity and capillary forces on the void profile. We are currently working to incorporate nucleation considerations into our void formation modeling to determine where in the chamber the shrinkage would initially appear before being displaced upward due to buoyancy. This information will be of vital importance when one must locate the void under microgravity conditions. Eventually such efforts should allow better prediction and control of the void patterns found in solidification processes involving PCMs, reducing the incidence of void-induced failures for a variety of phase change applications.

Conclusions

1) It is possible to include the effects of the capillary meniscus on the void profile during unidirectional solidification.

2) The influence of capillarity on the void profile is most pronounced at low values of the gravitational acceleration and for the special case of $\gamma = 0$.

3) The capillary solution also provides a characteristic length for sizing the final liquid reservoir, allowing a more realistic profile than previously possible.

4) The new capillary solutions are no longer scalable for container size and tend to Chalmers's result as the chamber height goes to infinity.

Appendix

All the comparisons discussed so far between Chalmers's solutions and the new capillary solutions have been based on a fixed container dimension H in both cases. As a result, the total mass of phase change material is slightly less for the capillary solution, because the presence of the capillary meniscus prevents the container from being initially filled with liquid to a depth of y or $z = H$ except along the walls. If a fixed PCM mass was instead specified for the two cases, then the corresponding H would have to be increased for the capillary solution.

The appropriate fixed-mass height H_{fm}, can easily be obtained from the specified PCM mass by solving the equations

$$\rho_l(H_{fm} - h)L + \rho_l A_{meniscus} = \text{Specified PCM mass/unit depth} \quad \text{(A1)}$$

for the Cartesian case and

$$\rho_l\pi(H_{fm} - h)R^2 + \rho_l V_{meniscus} = \text{Specified PCM mass} \quad \text{(A2)}$$

when considering radial solidification. Other than using $y(x = L)$ or $z(r = R) = H_{fm}$ instead of H as the initial condition, the capillary solidification analysis would proceed in exactly the same fashion as with a specified container size. Thus, the generalized Cartesian profiles from Eqs. (13) and (15) and the radial profiles from Eqs. (22) and (23) are still valid once H_{fm} is substituted for H. Similarly, the relevant dimensionless parameters and the fundamental behavior of the solutions would both remain unchanged.

Acknowledgments

This material is based upon work partly supported under C. D. Sulfredge's University of Kentucky Dissertation Year Fellowship. The project was also funded by the Air Force Aero Propulsion and Power Laboratory, Wright-Patterson Air Force Base, Dayton, Ohio, Contract F33615-87-C-2777.

References

[1]Chalmers, B., "How Water Freezes," *Scientific American*, Vol. 200, No. 2, 1959, pp. 114–122.

[2]Sulfredge, C. D., Chow, L. C., and Tagavi, K. A., "Void Formation in Radial Solidification of Cylinders," *Journal of Solar Energy Engineering*, Vol. 114, No. 1, Feb. 1992, pp. 32–39.

[3]Chalmers, B., *Principles of Solidification*, Wiley, New York, 1964, pp. 285–289.

[4]Tagavi, K. A., Chow, L. C., and Solaiappan, O., "Void Formation in Unidirectional Solidification in 1*g* and 0*g*," *Proceedings of the Workshop on the Commercialization of Space Fluid Management*, Univ. of Alabama, Huntsville, AL, 1990, pp. 254–270.

[5]Morris, D. G., Foote, J. P., and Olszewski, M., "Development of Encapsulated Lithium Hydride Thermal Energy Storage for Space Power Systems," Oak Ridge National Lab., ORNL/TM-10413, Oak Ridge, TN, 1987.

[6]Shamsundar, N., and Sparrow, E. M., "Effect of Density Change on Multidimensional Conduction Phase Change," *Journal of Heat Transfer*, Vol. 98, Nov. 1976, pp. 550–557.

[7]Wichner, R. P., Solomon, A. D., Drake, J. B., and Williams, P. T., "Thermal Analysis of Heat Storage Canisters for a Solar Dynamic Space Power System," *Proceedings of the 3rd International Conference on Solar Energy*, DE, 1987, pp. 319–328.

[8]Sulfredge, C. D., Chow, L. C., and Tagavi, K. A., "Solidification Void Formation in Tubes: Role of Liquid Shrinkage and Bubble Nucleation," *Experimental Heat Transfer*, Vol. 5, No. 3, 1992, pp. 149–162.

[9]Carey, V. P., *Liquid-Vapor Phase-Change Phenomena*, Hemisphere, Washington, DC, 1992, pp. 39, 40.

[10]Sulfredge, C. D., "Fundamentals of Solidification Shrinkage Void Formation," Ph.D. Dissertation, Univ. of Kentucky, Lexington, KY, 1993, p. 20.

[11]Swokowski, E. W., *Calculus with Analytic Geometry*, 3rd ed., Prindle, Weber and Schmidt, Boston, MA, 1984, p. 448.

[12]Ohno, A., *The Solidification of Metals*, Chijin Shokan Co., Ltd., Tokyo, Japan, 1976, pp. 126–130.